8-24-2011

Fabrication and Characterization of ZnO/CuO Core-Shell Nanowire Arrays

Kuo-ting Liao
UConn, kuo-ting.liao@huskymail.uconn.edu

Fabrication and Characterization of ZnO/CuO Core-Shell Nanowire Arrays

Kuo-Ting Liao

B.S., National Sun Yat-San University, 2007

A Thesis

Submitted in Partial Fulfillment of the

Requirements for the Degree of Master

at the

University of Connecticut

2010

APPROVAL PAGE

Master of Science Thesis

Fabrication and Characterization of ZnO/CuO Core-Shell Nanowire Arrays

Presented by

Kuo-Ting Liao, B.S.

Major Advisor _____

Puxian Gao

Associate Advisor _____

S. Pamir Alpay

Associate Advisor _____

Mei Wei

University of Connecticut

2010

ACKNOWLEGEMENTS

First of all, I would like to express my gratefulness to Professor Puxian Gao, my advisor, who directed me and supported me during my master's degree education. He helped me become familiar with nanomaterial research fields, and gave me advice when I struggled. From him, I learned the spirit of research—to be productive, patient, novel, and to never give up even when the experiments seem to fail at first.

I would also like to thank all the members in the Nanomaterial Science laboratory. They always showed full support in both scientific and personal ways. In particular, I would like to thank Mr. Paresh Shimpi, a senior student at the Nanomaterial Science laboratory. Paresh helped me to become familiar with all of the instruments when I first joined the laboratory and gave me some suggestions when I faced difficulties. He is also a very good friend who always cheers me up. In addition, I would like to thank all my dear friends here and in Taiwan. They picked me up when I was feeling down and continue to delight me all the time.

In the end, I would like to thank my family, who always support me mentally and materially. Without them, I might not have been able to finish my degree.

It is hard to express adequately my appreciation using only a piece of paper, but I still want to give my whole gratitude to all the people who always support me. Thank you.

Table of Content

List of Figures

Fabrication and Characterization of ZnO/CuO Core-shell Nanowire Arrays

Kuo-Ting Liao, M.S.

University of Connecticut, 2010

Research into nanomaterials has become more and more popular because of their unique properties compared to bulk materials. Amongst various functional materials, zinc oxide (ZnO), with a direct electron energy band gap of 3.34 eV at room temperature, is an important optoelectronic material with an intrinsically *n-type* semiconducting property. However, to form a *p-type* ZnO semiconductor is still a challenge. Copper oxide (CuO), compared to ZnO, has a much smaller band gap, 1.2 eV, and shows an intrinsically *p-type* semiconducting property. It has been suggested that when CuO is alloyed with ZnO properly, a *p-n* semiconductor heterojunction can be formed to be utilized in solar cell and gas sensor applications.

In this thesis, ZnO/CuO core-shell nanowire arrays have been successfully fabricated by a simple three-step process. ZnO nanowire arrays were first grown by the hydrothermal method using ZnO seeded substrates. Copper then was deposited on as-grown ZnO nanowire arrays by a DC sputtering method. Thermal oxidation of copper nanofilm was utilized to enable the formation of ZnO/CuO core-shell

nanowire arrays. The Cu nanofilm thermal oxidation behavior on the three-dimensional (3D) ZnO nanowire arrays was systematically studied by introducing different oxygen flows and different pressures. It has been suggested that increasing oxygen flow rate might increase local partial oxygen pressure, thereby increasing the degree of oxidation throughout each single ZnO/Cu core-shell nanowire. Higher pressure might favor the formation of Zn_2SiO_4 at the interface of ZnO and silicon substrates. ZnO/CuO core-shell nanowire arrays have exhibited better absorption efficiency in visible region as compared to the pure ZnO nanowire arrays, which suggests that ZnO/CuO core-shell nanowire arrays have strong potential as nanoscale building blocks in solar cells and light emission devices.

In this thesis layout, the first chapter gives general concepts and background on ZnO and CuO nanowires. Chapters 2 and 3 will provide the experimental methodologies and some important parameters to control. Chapter 4 focuses on the results and discussion on the characterization, growth mechanism, and Cu nanofilm oxidation behavior on 3D ZnO nanowire arrays. Chapter 5 concludes this thesis work and provides suggestions for the future work.

Chapter 1 Introduction

In this chapter, we will introduce background information and general concepts in nanomaterials. A few questions will be answered through the literature review, which include: What distinguishes nanomaterials from bulks? What is the advantage of nanomaterials? And what are the challenges of nanomaterial fabrication? Different low dimensional nanostructures will be introduced including ZnO and Cu_xO, which are the two materials studied in this thesis. In the end of this chapter, we will introduce the potential application of nanomaterials, especially in photovoltaics technology.

1.1 Nanotechnology

The concept of “nanotechnology” was first introduced in a famous talk given by Richard Feynman in 1959: “There's Plenty of Room at the Bottom.” In his talk, Dr. Feynman pointed out how scaling issues would affect many physical properties.[1] In the 1980s, Nano-based concepts had become more and more popular since there were some important nano-characterization instrumentation developments such as scanning tunneling microscope (STM), atomic force microscope (AFM), etc., which made it easier to study nanoscale materials. Since research on nanoscale materials became easier, nanotechnology has been expanding into several fields. For example, it plays

an important role in applications including biomaterial fields [2, 3] and solar devices [4]. The properties, such as electronic, optical, and chemical characteristics of nanoscale materials are distinct from those of bulk materials [5]. In the following section, we will introduce the nanomaterials' advantages and their challenges.

1.2 Nanomaterials

Nanomaterials typically refer to the materials which have at least one dimension in nanometer scale (~0.1-100 nm). Because of their nanoscale, nanomaterials have relatively large surface area which might result in different properties from bulks. For example, due to a huge fraction of surface atoms, nanomaterials may have lower melting point compared to the bulks. Also, for electrical properties, nanomaterials tend to have reduced conductivity than the bulks because of increasing surface scattering. However, conductivity of nanomaterials sometimes can also be increased by doping with different elements.[6] The following subsection will introduce nanomaterials with different morphologies, especially one dimensional nanorods, nanowires, and core-shell nanostructure.

1.2.1 One Dimensional Nanostructures

In 1991, a Japanese researcher, Sumio Iijima, discovered nanotubes at NEC, which brought more attention to the one dimensional nanostructures due to their

distinct properties from bulks or three-dimensional (3D) materials.[7] These one dimensional nanostructures have diameters range from one nanometer to hundreds of nanometer. Nanorods and nanowires are all considered as one dimensional nanostructures, but nanorods generally have much smaller aspect ratio than nanowires. For one dimensional nanostructures, they normally present with specific axial direction. In this thesis, we will mainly focus on nanowires. Nanowires play an important role in nanodevices fabrication as a result of their unique electronic transport, optical, and other properties because of quantum confinement effect. [8] Many different elements or compounds have been synthesized successfully to form nanowires. For example, gallium nitrite, silicon, zinc magnesium, copper oxide, and zinc oxide nanowires. There are several ways to fabricate nanowires, such as template based method, chemical vapor deposition[9], laser ablation[10], and solution based method[11]. More details will be introduced in the following sections.

1.2.2 Core-Shell Structure

Recently, core-shell nanowires have brought much attention because of the possibility to tune the properties of core nanocrystal with addition of the shell. By choosing appropriate core and shell materials, the emission wavelength can be tuned in a larger range than both of materials alone. For example, it will lead to enhancement of blue shifted near band edge UV emission when MgO/ZnO nanowires

arrays are formed. [12]

Based on different band structure alignment at core and shell materials' interface, there are three different systems, type I, type II, and type III. At Type I, band gap of shell materials is larger than that of core materials, in which electrons and holes will be confined within core materials. At type II, band gap of shell materials is smaller than that of core materials, in which electrons and holes will be partially or completely confined within shell depending on how thick shell materials is. At type III, either the valence-band edge or the conduction band edge of the shell material is located in the band gap of the core.

Here we will focus on type II. In type II systems, smaller band gap material is deposited onto larger band gap materials. Charge carriers are at least partially delocalized in the shell and the emission wavelength can be tuned by the different thickness of shell materials. Generally, a significant red-shift of the band gap with the shell thickness is observed.[13] This type of core-shell structure is assumed to give a tunable band gap range that exceeds the one that conventional alloy formed. The lower limit of band gap can be substantially lower than lower band gap materials, while upper limit of band gap will be close to larger band gap materials.[14] Also, core material and shell material should be crystallized in similar structure so that the lattice mismatch can be small.[13]

1.2.3 Zinc Oxide and Copper Oxide

The materials that this thesis is focused on are zinc oxide and copper oxide. Zinc oxide, ZnO, can be fabricated in different nanoscale morphologies including nanowires, nanobelts, and nanodendrites.[15] It can also be doped by different materials to enhance its properties. For example, doping magnesium into ZnO nanowires can enhance its UV optical properties.[12] Copper oxide, CuO or Cu_2O, has been widely used in semiconductor industry. The ease to get raw source for this material has brought up a lot of interests in investigating these materials.

1.2.3.1 ZnO

ZnO is a direct band gap material with a band gap around 3.3 eV at 300K. It has a large exciton binding energy of 60meV. ZnO is considered as a II-VI semiconductor. Like most of II-VI semiconductors, ZnO has three types of crystal structures, rocksalt, zincblende, and wurtzite. Rocksalt structure will only appear at a relatively high pressure environment. Zinc blende structure can be achieved by growing ZnO onto substrates which are cubic structure. Normally at room temperature, it will stay in wurtzite structure, which is thermodynamically more stable.[16] Wurtzite structure has hexagonal unit cell (space group P63mc) with zinc hexagonal sublattice and oxygen hexagonal sublattice stacking together. In the unit

cell, Zn^{2+} and O^{2-} ions are located at tetragonal sites which are surrounded by other kind of ions. (0001) plane is the close-packing plane with atomic stacking sequence ABABAB along [0001] direction.

Due to different electronegativity between two ions, polar Zn-O bond appears which results in positively Zn^{2+} (0001) and negatively O^{2-}(000-1) planes. This polarity can affect many material properties, such as spontaneous polarization and piezoelectricity. ZnO is well known to exhibit anisotropic growth.[17] In ZnO wurtzite structure, most common growth direction is alone [0001] direction with a few other secondary growth directions such as [2-1-10] and [01-10]. [16, 18]

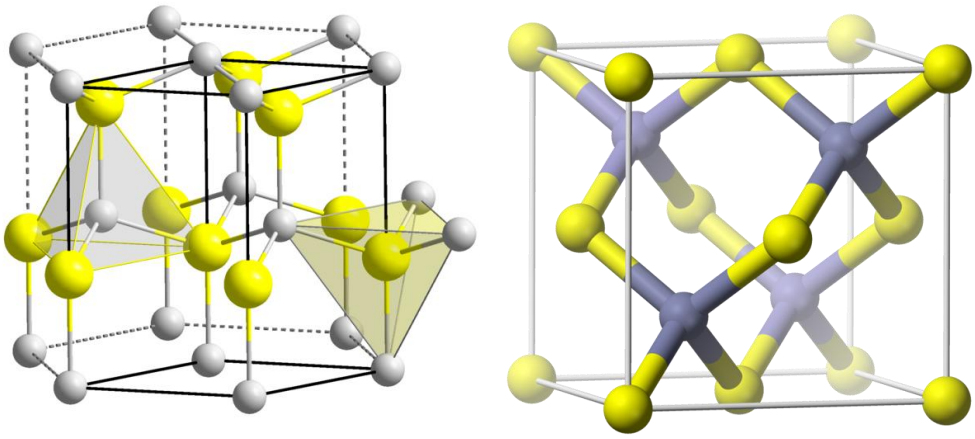

Figure 1 The crystal structure of ZnO. Left: Wurtzite structure, Right: Zinc blend unit cell. (Reproduced from wikipedia.org)

ZnO normally has a *n-type* semiconducting property even without doping, while *p-type* doping in ZnO still remains a challenge. However, it does not diminish the interests in using ZnO for electronic and optoelectronic applications. Many alternative methods have been applied to solve this problem. Heterostructured *p-n* junction is

most common one.[16, 19] Recently, the effect of alloying on ZnO based nanostructures has brought attention great deal attention because of its potential to improve its electrical, optical and other functional properties. Many different binary systems, such as MgO/ZnO [12], Cu/ZnO [20]and Co/ZnO[21], have been done for different applications. It has been suggested that alloying Cu_xO into ZnO can help form the *p-n* junction, which can be utilized in solar and gas sensors applications [22-24].

1.2.3.2 Cu_xO

Copper oxide has two types of polymorphism, cuprous oxide (Cu_2O) and cupric oxide (CuO). Color, structure, and physical properties of these two forms are different. Cu_2O is a compound with either red or yellow color, whose crystal structure is cubic (space group Pn-3m). Cu^+ ions occupy face-center sublattice and O^{2-} ions form body-center sublattice. Cu_2O is a direct band gap material with a band gap around 2.0 eV and it has a *p-type* semiconducting property. Absorption efficiency in the visible region and electrical properties are good for Cu_2O, which enables a good candidate for photovoltaic applications. [14, 25]CuO appears black with its crystal structure more complicated monoclinic tenorite structure (space group 2/m). The Cu^{2+} ions are at centers of inversion symmetry in a single four-fold site 4c (1/4, 1/4, 0) and the oxygen ions occupy a four-fold set 4e (0, y, 1/4). CuO is a narrow band gap material with a band gap around 1.2 eV, and it also has a *p-type* semiconducting property.

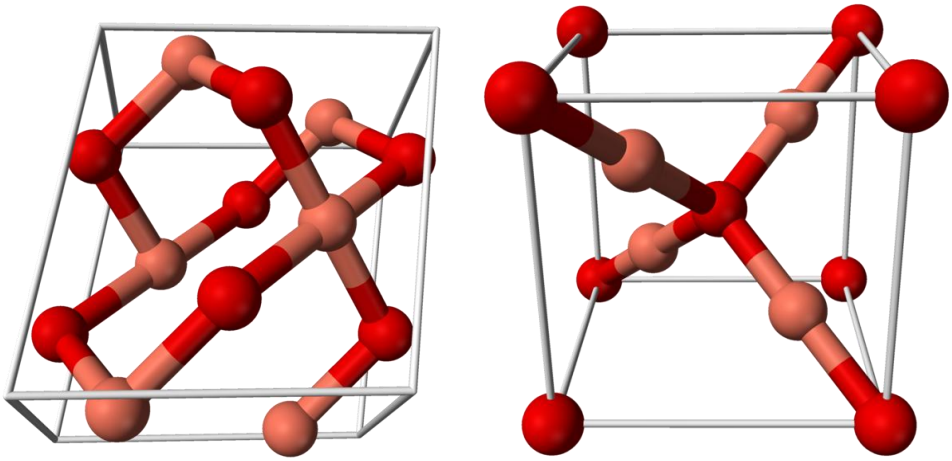

Figure 2 Crystal structure of Left: CuO, monoclinic stucture. Right: Cu_2O, Cubic structure.(Reproduced from wikipedia.org)

Copper oxide intrinsically is a *p-type* semiconductor because of Copper vacancies or Oxygen interstitials. Both Cu_2O and CuO draw much attention since the starting material Cu is inexpensive and easy to get, and the methods to prepare these materials are of low cost. There are many methods of fabricating Cu_2O and CuO, such as thermal oxidation, chemical vapor deposition, etc. It is easy to form a mixture phase of Cu_2O and CuO under an ambient environment; therefore, how to maintain phase purity becomes one of the major issues to fabricate these materials.[25-27]

1.3 Applications

Nanomaterials have several applications. It ranges from electronics, biological systems to optical communications. Because there are so many devices that have been fabricated, it is impossible to list all of them. This section will focus on introducing photovoltaic devices based on nanomaterials[28].

1.3.1 Photovoltaic Devices

A solar cell is a device that coverts sun light into electricity by photovoltaic effect. Because of its renewable and energy conversion properties, it becomes more and more popular [29]. Several different technology approaches have been used to build the solar devices, such as thin film solar cells [30],and dye-sensitized solar cells [31]. Recently, low dimensional nanostructure have brought up much attention to fabricate photovoltaic devices.[22] Using nanostructure materials can improve not only efficiency but reduce the cost and size. Among all the available nanostructure, recently, core-shell semiconductor nanowires have gained a lot of interests. Comparing to conventional solar cells, core-shell structure solar cells have several advantages. For example, for conventional solar cells, electrons and holes stay in same region after photoexcitation, so electrons and holes have larger chance to recombine again, which will decrease electronic transport efficiency. [14] However, core-shell structure photovoltaic devices have greater carrier collection and overall efficiency because each core-shell nanostructure might have high aspect ratio which allows optimal light absorption and carrier extraction into orthogonal spatial directions.[32] Core-shell nanowire arrays can help to direct carriers in one direction, which decreases random walk of charge carriers. However, to achieve homogeneous *p-n* junction oxide semiconductors simultaneously is difficult, which allows the heterostructured *p-n*

junction to potentially thrive given much more flexible choices of dissimilar semiconductors just like Cu_xO and ZnO.

1.4 Thesis Structure

To summarize, this thesis will focus on synthesis, characterization, and result discussion of ZnO/CuO core-shell nanowire arrays. In this opening chapter, we introduce some background concepts in nanotechnology, nanostructure, materials, and photovoltaic applications. In the following chapter, we will introduce relevant nanomaterials synthesis; growth mechanisms, and experimental methodologies used in this thesis work.

Chapter 2: Synthesis, Growth Mechanisms, and Experimental Methodologies

As mentioned in previous section, there are many ways to synthesize 1D nanostructure. At the first section of this chapter, three main synthesis methods will be introduced, including solution based methods, physical vapor deposition, and chemical vapor deposition. At the second section, general growth mechanisms will be introduced, and in the end of the chapter, experimental methodologies for this thesis work will be introduced.

2.1 Synthesis

There are many synthesis methods for low-dimensional nanostructures. It can be divided into two main routes: top-down and bottom-up. In nanoscale materials synthesis, the bottom-up approach is more commonly used, since the top-down approach normally will introduce internal stress and potentially influence (modify or damage) on the nanomaterials' crystal structures and introduce impurities.[6] The following subsections will introduce three main approaches including chemical vapor deposition, physical vapor deposition, and solution based methods.

2.1.1 Physical Vapor Deposition

Physical vapor deposition (PVD) is a process to deposit materials onto substrates without a chemical reaction. Typically, it can be divided into two main categories, evaporation and sputtering. There are some differences between these two. For example, evaporation is a thermodynamically equilibrium process, whereas sputtering is not. Also, evaporation will form relatively larger grain size thin films with worse adhesion to substrates than sputtering. Here we will focus on introduce the sputtering process. Sputtering is a process that high energy ions bump into the target and release surface atoms from the target because of momentum exchange between the ions and atoms.[33] There are several ways to generate energetic ions, such as by plasma or ion sources. Different targets might have different sputtering rates, but generally, sputtering is less time consuming than a spin coating process. Another advantage is sputtering is environmentally friendly, simple, stable and an easily controlled deposition procedure.[34]

2.1.2 Chemical Vapor Deposition

Another way to fabricate nanostructure is chemical vapor deposition (CVD). CVD is a chemical process that chemical reactants react in gas phase and form solid products. It was first used in 1983 by de Lodyguine [35]. Many different forms of CVD

have been found in literatures, such as metal organic chemical vapor deposition (MOCVD), and Plasma enhanced chemical vapor deposition (PECVD). There are several advantages of CVD. Using a CVD process, it can produce high purity and density materials. Also, by controlling CVD parameters, it is possible to control crystal structure, surface morphologies and orientation of CVD products. For example, ZnS has been successfully fabricated in different morphologies by CVD.[36] However, there are also some disadvantages for this technique. For example, it is difficult to deposit multiple components since every element has its own evaporation rate. Moreover, CVD costs more than solution base methods.[37]

2.1.3 Solution Based Methods

In many cases, a chemical reaction only takes place in solution. To control experiment parameters, such as temperature, precursors, changing of pH value and capping reagents, etc., it is possible to manipulate and control different morphologies.[38] The advantage of solution based methods is that the nanostructure can be synthesized at a relatively low temperature (<350℃) compared to vapor phase synthesis, which can eliminate or reduce the limitation of substrates choices. Also, it has potential to fabricate uniform and high density nanostructure. Depending on precursors, solution based methods can be of relatively low cost. For example, hydrothermal synthesis is a well-known low cost method to fabricate oriented and

high density ZnO nanowire arrays.[39] However, there are some disadvantages of this synthesis method. One of the major disadvantages is the hard-to-control parameters' variation or noises during the experimental processes. In addition, more defects tend to be generated than the vapor phase deposition. This thesis will be focusing on using solution based methods for ZnO nanowire growth.

2.2 Growth Mechanisms

The Growth mechanisms of this thesis are split into two parts. First part is the formation of ZnO nanowires by solution based methods. Second part is the formation of Cu_xO by thermal oxidation.

2.2.1 Formation of Nanowires

Since nanowires could have distinct physical and chemical properties from bulk materials, it has become a promising class of nanomaterials for many structural and functional applications. Therefore, to understand the nanowire growth mechanism and how to control the growth process has been an important research focus lately. In general, nanowires are formed because they have a tendency to grow or crystallize along a specific direction. That is, the facet with higher surface energy tends to grow faster than the others assuming a crystal form nanowire. In general, it is a crystal growth process in order to reduce the total Gibbs free energy in the materials system.

Several steps could happen in a sequential order in solution based methods. First, the precursor dissolves and diffuses onto the growth surface. Second, adsorption and desorption of the precursor from the growth surface. Third, surface diffusion takes place, in which precursors might contribute to crystal growth or escape from the surface. During surface growth, a supersaturation or high concentration of precursors will determine the growth rate. High concentration might also result in secondary nucleation, which might cause end of single crystal growth. [6] However, using solution based methods, it is relatively harder to achieve high aspect ratio nanowires than vapor based methods. In this thesis, ZnO thin seed layer has been used to grow well-align and small diameter ZnO nanowires[40].

2.2.2 Formation of Cu_xO

To form the core-shell structure, thermal oxidation has been used to form Cu_xO shell. Thermal oxidation is a process to produce oxide products. Most of the processes are conducted in furnaces. Thermal oxidation can be applied to many different materials. Taking copper oxide as an example, at a high temperature thermal oxidation process (>600℃), the formation of oxide scales on Cu involves migration of electrons and cations to the local reaction zone. Literatures show that to form copper oxide, it is copper ions diffusing instead of oxides.[41, 42] At a low temperature thermal oxidation process, oxygen pressure and temperature are relatively insensitive for reaction rate. A

low temperature (<300°C) thermal oxidation process can yield uniform copper oxide thin film.[43] However, for the '[process that is carried between 275℃ to 970℃, Cu_2O first forms and then transforms into CuO, depending on reaction time and temperature.[44] In addition, thin film and bulk Cu have different oxidation mechanisms. For bulk Cu, the preferential oxidation planes are (100), (111), (110), and growth is driven by copper ions concentration gradient [72]. For thin film Cu, it is found that Cu^+ is dominant below 275℃, while Cu^{2+} becomes dominant at temperature above 275℃, which disagrees with the thermodynamic stability calculation.[41, 45] Further details will be discussed later in section 4.2.

2.3 Experimental Methodologies

The Experimental methodologies include two parts. One is the set-up for nanomaterials synthesis. The other is the characterization methods of nanomaterials.

2.3.1 Synthesis Equipments

In this thesis, a ZnO seed layer is first sputtered onto a silicon substrate by RF sputtering (Torr CRC-632). Then, ZnO nanowires are grown by a hydrothermal process, which is carried out in an isotemperature digital-control water Bath. Finally, thermal oxidation is carried out in a low pressure vapor deposition system, which consists of a rotary pump, a gas mass flow meter, a water cooling system and a high

temperature tube furnace. The substrate is put at the center of furnace on the alumina boat. After prepumping to a certain vacuum level, thermal oxidation is conducted by setting two types of parameters. One is thermodynamic parameters such as temperature and pressure, the other is kinetic parameters such as duration time, ramping rate, and oxygen flow rate. In this thesis, different sets of parameters have been used for the experiments, and experimental details will be presented in section 3.2.

2.3.2 Characterization Methods

To investigate in morphologies, structure, and optical properties, several instruments have been used. A JEOL JSM 6335F field emission scanning electron microscope (SEM), a FEI Tecnai 12 scanning transmission electron microscope (STEM), and a JEOL 2010 high resolution TEM were used to characterize nanostructural morphologies and crystal structure. Energy dispersive x-ray spectrometers (EDXS) attached to the SEM and TEM, and a BRUKER AXS D5005 (Cu Kα radiation, $\lambda = 1.540\ 598$ A°) x-ray diffractometer (XRD) were used to determine the compositions and phase structure of samples, respectively. A Cary 5000 UV-visible spectrometer was used to investigate the optical properties of nanostructure.

2.4 Summary

In this chapter, several synthesis methods have been first introduced. Growth mechanisms for ZnO nanowires and Cu_xO are explained briefly. Finally, the equipments and instruments that are used to synthesize and characterize the nanomaterials in this thesis have been summarized. In the following chapters, experimental procedures, results and conclusions will be illustrated based on the techniques, growth mechanisms and information that have been introduced in this chapter.

Chapter 3: Fabrication of ZnO/Cu_xO Nanowire Arrays

As stated earlier, this thesis is focusing on Cu_xO/ZnO heterostuctured nanowire arrays. In this chapter, we will first briefly introduce the general background information for fabrication of Cu_xO/ZnO heterostuctured nanowire arrays, following by experimental procedures, and then the effect of using seed layers and annealing processes will be discussed.

3.1 Introduction

Since the discovery of first carbon nanotube, much one-dimensional nanostructure has been successfully fabricated, including nanowires, nanorods, and nanobelts.[20] Among those structure, ZnO nanowires have been a promising class of nanomaterials for electronic and optical applications due to its wide band gap (3.3 eV), large exciton binding energy (60 meV), and good chemical and thermal stability.[46] To fabricate ZnO based optoelectronic devices, one can dope ZnO with different elements to achieve *p-n* junction. Copper oxide has been used for doping in ZnO to form *p-n* heterojunctions.[47, 48] Copper oxide, as mentioned in previous chapter, can be either CuO with a band gap of 1.2 eV or Cu_2O with a band gap of 2.0 eV. They are both

p-type semiconductors. On the other hand, as a starting material, copper is easy and cheap to get on earth, therefore many people start to investigate Cu_xO based heterostructure. Theoretically, Cu_2O/ ZnO heterostructured nanowire arrays could achieve 20% solar energy conversion efficiency.[49] However, due to poor crystallinity, the efficiency is still much lower than the theoretic value.[50] In this thesis, a three-step synthesis process has been used to fabricate Cu_xO/ZnO heterostructure nanowire arrays.

3.2 **Experimental Procedure**

In this study, ZnO/Cu_xO heterostructure nanowire arrays have been grown on a Si substrate by a three-step process, as schemed in Figure 3. 30nm ZnO seed layer was first deposited on a Si substrate by RF Sputtering. After annealing the seeded substrate at 200℃ for 30 minutes, ZnO nanowire arrays were grown on those seeded substrate by a well-known hydrothermal method. For precursor solution p reparation, we mixed zinc nitrite hexahydrate ($Zn(NO_3)_2 \cdot 6H_2O$) and hexamethylenetetramine (HMT) with one to one molar ratio in the de-ionized water at 80℃. Chemical reactions took place as follow:

(1) $C_6H_{12}N_4+6H_2O \rightarrow 4NH_3+6HCHO$

(2) $NH_3+H_2O \rightarrow NH_4^+ + OH^-$

(3) $Zn^{2+}+2OH^{-} \leftarrow\rightarrow Zn(OH)_2$

(4) $Zn(OH)_2 \leftarrow\rightarrow ZnO+H_2O$

As mentioned in the previous chapter, when concentration of precursor becomes higher, nucleation will occur. That is, when ZnO concentration in aqueous solution becomes saturated, individual ZnO crystal nucleates and begins to grow along c-axis and evolves into a nanowire. The formed ZnO nanowire arrays were sputter-coated with 20nm Cu nanofilm, forming ZnO/Cu core-shell nanowire arrays. The desired ZnO/Cu_xO core-shell nanowire arrays were formed by annealing the Cu-ZnO nanowire arrays with and without oxygen flow.

During the experiment, different oxygen flow rates (20sccm, 50sccm, and 80sccm) and pressure (100mbar and 500mbar, 1atm) were used. Scanning Electron Microscope (SEM), Transmission Electron microscope (TEM), X-ray diffraction (XRD), UV-visible spectroscopy and Photoluminesence(PL) were used to characterize morphologies, structure, and optical properties.

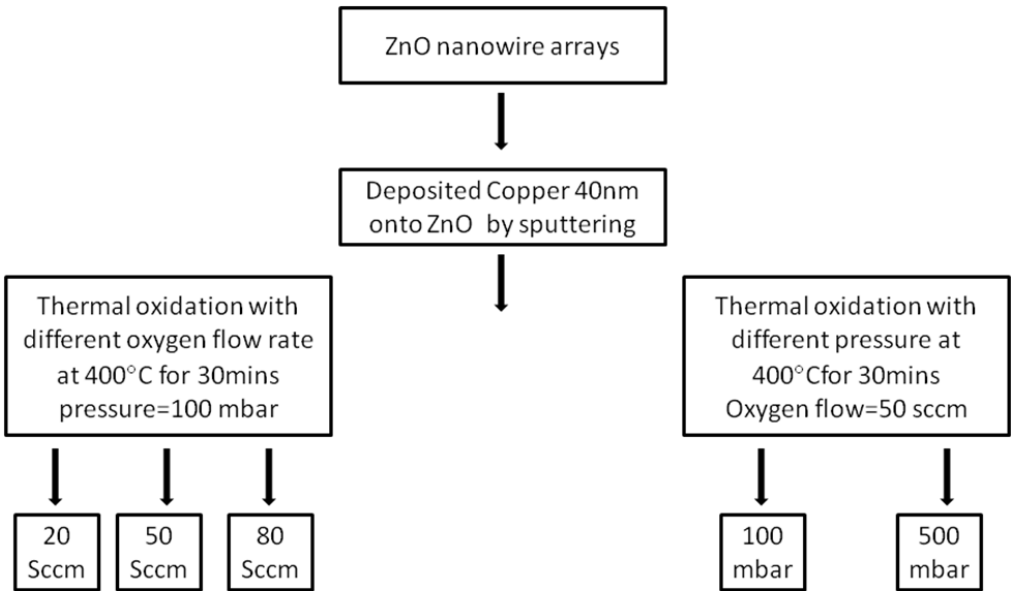

Figure 3. Experimental procedures for synthesizing ZnO/CuO core-shell nanowire arrays.

3.3 Experimental Factors

There are many factors that may affect the growth of ZnO nanowire, such as growth temperature, duration time, precursor concentration, capping agenst, and seed layers. From literature reviews, it shows that nanowires morphologies and aspect ratios are more related to growth temperature and duration time. Precursor concentration will also affect aspect ratios and the density of nanowires.[51] Here, we will focus on discussing how seed layers will affect the growth of ZnO nanowires.

3.3.1 Effect of Seed Layers

There are some methods to prepare seed layer. Spin coating and RF sputtering are commonly used ones.[52] By introducing a seed layer, ZnO nanowires can achieve

high quality along c-axis. Au and ZnO had both been used as seed layers to grow well-aligned ZnO nanowires.[53] Different characteristics of seed layers such as thickness of seed layers and a preaanealing process will result in different quality of ZnO nanowires. [54] For instance, we have found that comparing the ZnO nanowires growth on 200 nm thick seeds and 50 nm thick seeds, the growth on 50 nm thick seeds is much more uniform in terms of nanowire's diameter distribution, as shown in Figure 4.

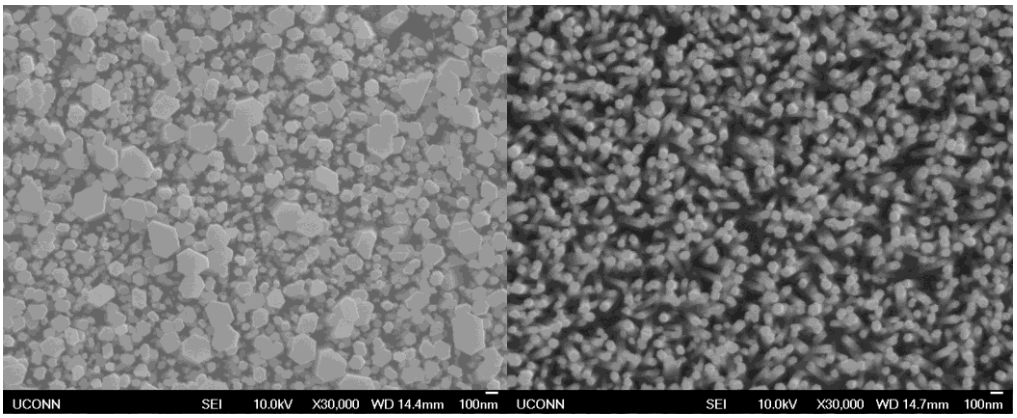

Figure 4. *Top view SEM images Left: ZnO nanowires grown by a hydrothermal method with 200nm seed layer preseeded. Right :ZnO nanowires grown by a hydrothermal method with 200nm seed layer presented.*

3.3.2 Effect of Annealing Processes

An annealing process is a heat treatment process which can reduce internal stress, and improve crystallinity. By pre-annealing the seed layer, the uniformity of the nanoscale grain diameter and crystallinity of the seed layer can be improved. Figure 5 compares the ZnO nanowires grown from a pre-annealing seed layer and the one without a pre-annealing process, which clearly suggested the improvement of

nanowires quality on a annealed seed layer.

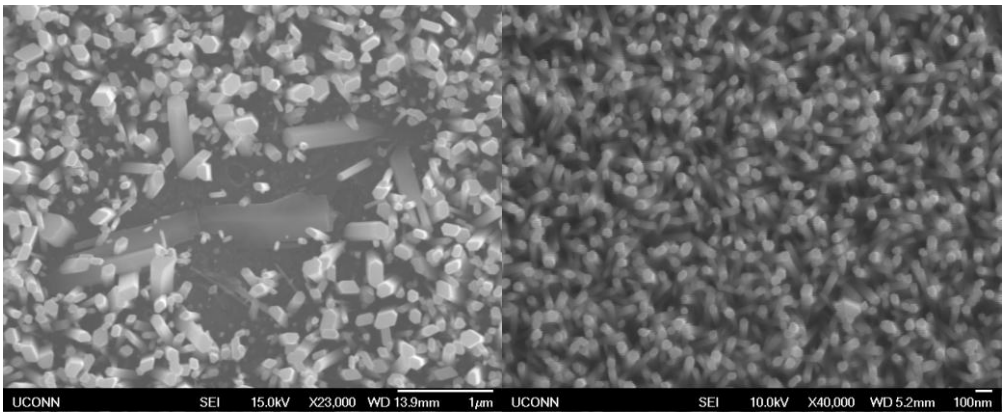

Figure 5. *Top view SEM images Left: ZnO nanowires grown by a hydrothermal method on pre-annealed seeded substrates. Right: ZnO nanowires grown by a hydrothermal method on seeded substrates without a pre-annealing treatment. ZnO nanowires grown on pre-annealed seeded substrates and non-annealed seeded substrate. Left: a non-annealed substrate; Right: an annealed substrate.*

It is clear that a pre-annealed substrate can help grow more uniform and better distribution nanowires than the substrate without a pre-annealing process. In addition, different annealing parameters will affect the characteristics of grown ZnO nanowires. Figure 6 illustrates the different characteristic ZnO nanowires grown from the seed layers with different pre-annealing times.

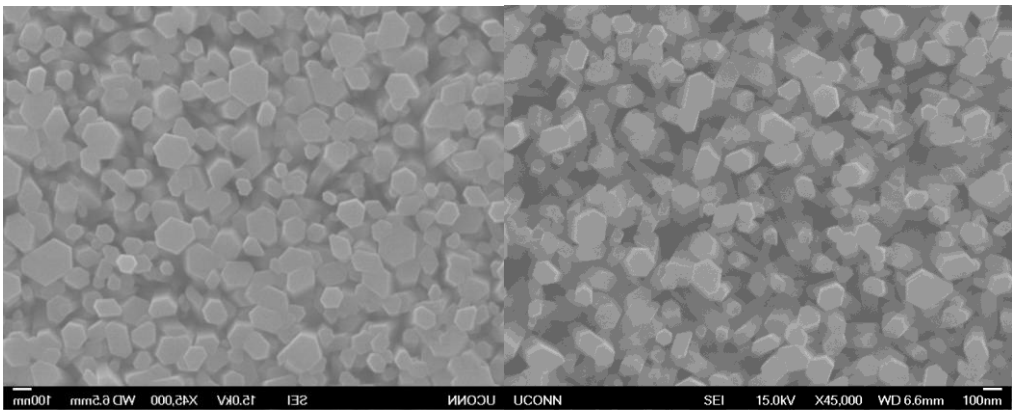

Figure 6. *Top view SEM images Left: ZnO nanowires grown by a hydrothermal method on 15 mins pre-annealed seeded substrates. Right: ZnO nanowires grown by a hydrothermal method on 1hr pre-annealed seeded substrates.*

3.4. Discussion of Pretreatment effects

Previous section indicates that the size, density and quality of grown ZnO nanowires in hydrothermal synthesis were highly related to the pretreatment of seed layers. When a pre-annealing process was conducted for longer time and higher temperature, the grains in the seed layer accumulated more energy to realign and merge themselves into larger seed islands in order to reduce the surface energy, which therefore might result in the growth of nanowires with larger diameter, less density, and higher crystallinity.

However, while a seed layer became thicker, under the same pre-annealing condition, the same amount of thermal energy might not be enough to enable every single nanograin to realign and merge with other grains. In other word, only some of those nanograins will agglomerate and form larger grains, resulting in much more diverse size-distribution and a poor alignment. [73-75]

3.5 Summary

In this chapter, fabrication of ZnO/Cu_xO core-shell nanowire arrays has been introduced. Experimental details have been demonstrated first and some factors that might affect ZnO nanowires growth have been discussed later. In the next chapter, we

will introduce the results and discussions on the characterized physical properties of ZnO/Cu_xO core-shell nanowire arrays.

Chapter 4: Physical Properties and Effective Factors of ZnO/Cu_xO Core-shell Nanowire Arrays

In this chapter, physical properties of ZnO/Cu_xO core-shell nanowire arrays will be discussed. Specifically, we will discuss the morphologies of ZnO/Cu_xO core-shell nanowire arrays first, and then analyze the characterized structural properties of ZnO/Cu_xO core-shell nanowire arrays. Finally, optical and electrical properties of nanowire arrays will be discussed.

4.1 Characterization oF ZnO/Cu_xO Core-shell Nanowire Arrays

In this section, the characterized physical properties of ZnO/Cu_xO nanowire arrays will be discussed. We will first introduce the observation by visible eye, and move to SEM results. Finally, we will discuss TEM results for the grown ZnO and ZnO/Cu_xO nanowire arrays.

4.1.1 Visible Observation

In this work, different oxygen flow rates and the pressures have been used during

the growth experiments, which result in samples with different visible colors. Sample a is in the 100mbar pressure with 20 sccm oxygen flow and sample e is in the 500mbar pressure with 50 sccm oxygen flow, and both samples appear yellow color. Sample b is in the 100mbar pressure with 50 sccm oxygen flow and sample d is in the 100mbar pressure without oxygen flow. Both samples appear black color. Sample c is in 100mbar pressure with 80 sccm oxygen flow. This sample appears shiny green and bronze color at some parts.

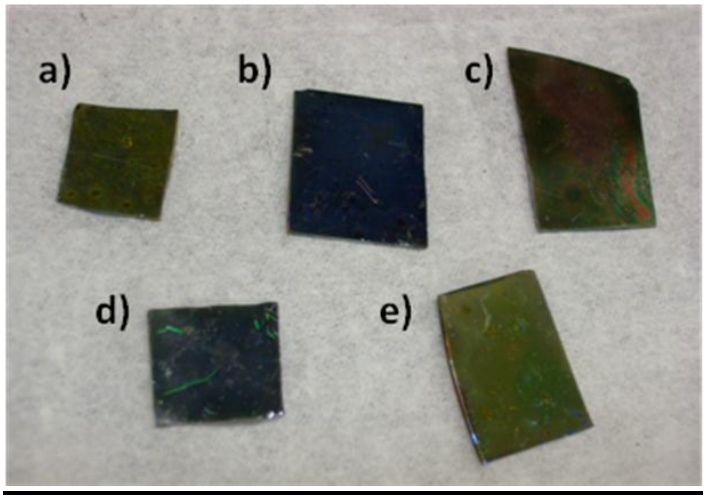

Figure 7. *Visible observation of the color change from samples under different synthesizing condition, a) Sample 1(S1) grown under pressure 100mbar with 20sccm oxygen introducing. b)Sample 2(S2) grown under pressure 100mbar with 50sccm oxygen introducing. c) Sample 3(S3) grown under pressure 100mbar with 80sccm oxygen introducing. d) Sample1 0(S0) grown under pressure 100mbar without oxygen introducing.e)Sample 4(S4) grown under pressure 500mbar with 50sccm oxygen introducing.*

As mentioned before, Cu_2O appears either red or yellow in color, while CuO

appears black in color so that the color difference at the surface might be due to different compositions in these samples. Further discussion will be brought in the following sections.

4.1.2 SEM and EDX

This section will show the results obtained under scanning electron microscope. As the previous section mentioned, ZnO was first deposited onto silicon substrates following by sputtering the Cu onto ZnO nanowires. Figure 8 shows the Cu/ZnO nanowires after sputtering 20nm thick Cu film. It shows that after depositing Cu onto ZnO nanowires substrates, the Cu/ ZnO nanowires are approximately 80nm to 110nm in diameter, ~300- 600nm long. From the tilt view, these nanowires have the nail-shaped structure.

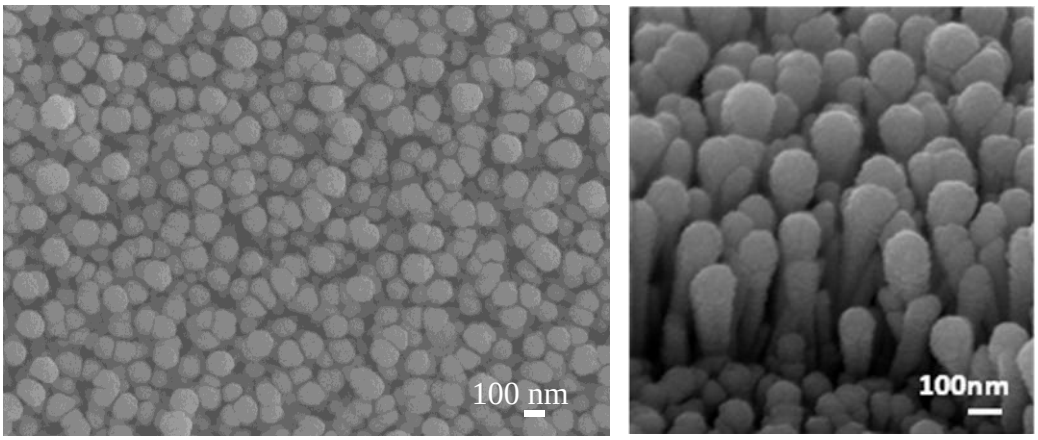

Figure 8. *Left :Top view SEM image of ZnO-Cu core-shell nanowires after deposition of 20nm Cu film; Right: 30° tilt view SEM image of the Cu/ZnO nanowires' nail-shaped structure.*

Table I. A list of 5 typical ZnO/Cu_xO core-shell nanowire arrays samples (S1, S2,…, S0) after various annealing processes with variable pressure and oxygen flow

rates.

	Temperature	Pressure	Oxygen flow	Core-shell
S1	400℃	100 mbar	20sccm	poor
S2	400℃	100mbar	50sccm	good
S3	400℃	100mbar	80sccm	poor
S4	400℃	500mbar	50sccm	poor
S0	400℃	100mbar	no	ok

Figure 9 a-d show the ZnO/Cu_xO core-shell nanowire arrays formed at different growth conditions. The comparison of top view SEM images suggests that the larger the oxygen flow rate, the more CuO rich regions formed on top of the nanowires. The nanowire arrays became more close-packed in a higher oxygen flow rate than in the lower one. For S4, which was under pressure 500mbar, the oxygen partial pressure should be higher than any other cases which resulted in flat Cu_xO thin film on top of ZnO nanowire arrays. The inset figure is a 30° tilt view SEM image which further illustrates the formed Cu_xO distribution throughout the entire ZnO nanowire arrays.

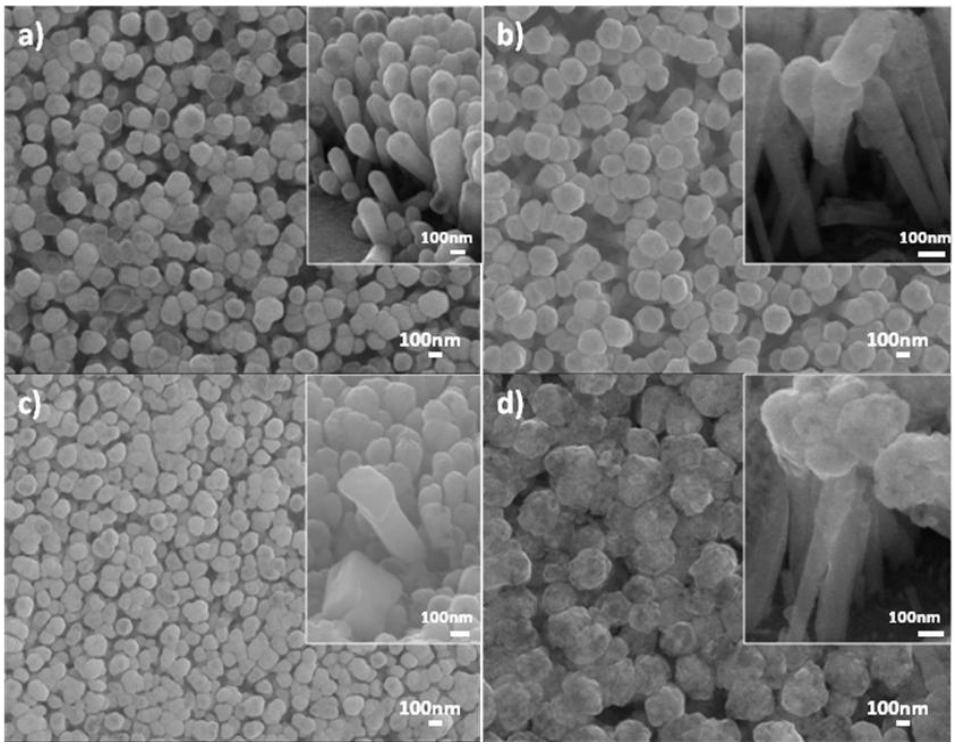

Figure 9. *ZnO-CuO core-shell nanowires formed by annealing ZnO-Cu core-shell nanowires at 400 ^{0}C for 1 hour with different pressure and oxygen flow rates. (a) Top view SEM image of sample S0: without oxygen flow and 100mbar pressure. Inset showing distinction between the tip and body region and their EDXS composition difference on the right showing higher copper concentration on the tip region. (b) Top view SEM image of sample S1: 20sccm oxygen flow and 100mbar pressure. (c) Top view SEM image of Sample S2: 50sccm oxygen flow rate, 100mbar pressure and has good-conformal coating of the shell layer compared to any other sample. (d) Top view SEM image of sample S3: 80sccm oxygen flow rate and 100mabr pressure. (e) Top view SEM image and inset of sample S4: 50sccm oxygen flow rate and 500mbar pressure.*

Figure 10 shows Cu, O, and Zn exist from EDX result. From the tilt view and composition analysis in EDX, it also indicates that Cu content was high at the tip part, which suggests that CuO accumulated on the top of ZnO/CuO core-shell nanowire arrays.

Atom%				
	O-K	Si-K	Cu-K	Zn-K
Tip	46.76	14.37	18.62	19.72
Body	32.89	26.92	5.28	34.91

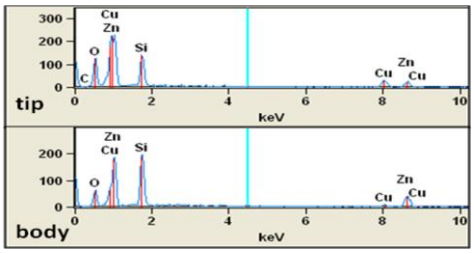

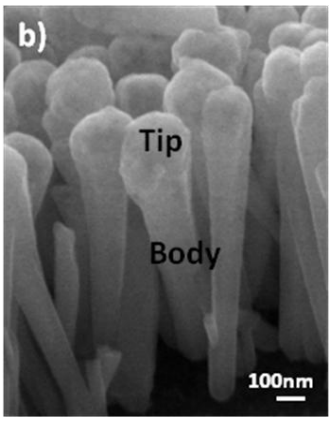

Figure 10. a)EDX showing composition analysis of this CuO/ZnO core-shell nanowire arrays b)30° SEM tilt view image of CuO/ZnO core-shell nanowire arrays formed after thermal annealing under pressure 100mbar with no oxygen introducing.

4.1.3 TEM

This section will introduce TEM results. Figure 11 shows the images of Cu deposit onto ZnO nanowire arrays. It shows that copper tended to deposit on ZnO nanowire as a small particle. Also from the TEM image, copper thoroughly deposited onto the entire ZnO nanowire.

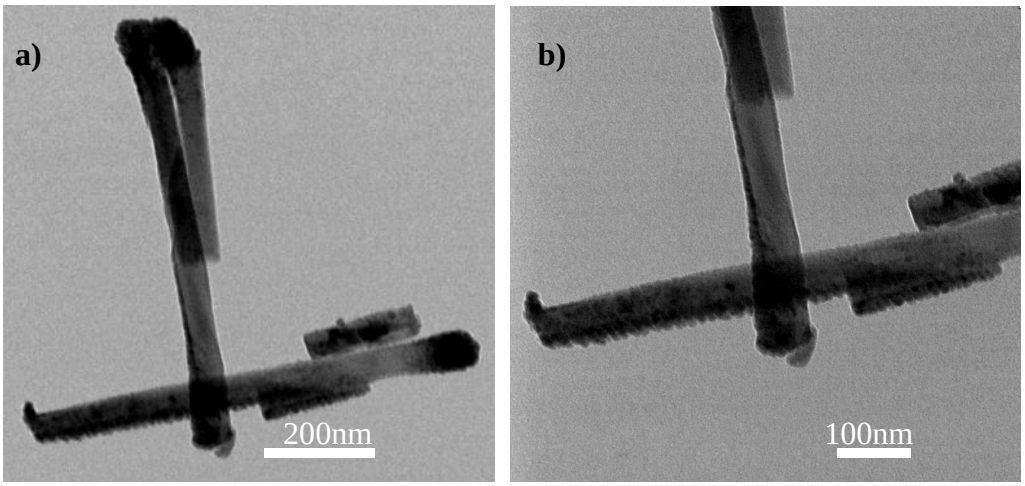

Figure 11. *TEM images of a) As-deposit 20nm Cu onto ZnO nanowire arrays. b)* Zoom-in *TEM image of bottom portion.*

After thermal oxidation, CuO shell formed around ZnO core. Depending on different growing condition, the quality of core-shell nanowires is different. Figure 12

shows the TEM result of a ZnO/CuO core-shell nanowire grown at 400 ℃, 100 mbar without oxygen flow. Figure 12 a) and b) show the bright field and dark field TEM images of a core-shell nanowire, respectively. It can see that CuO covered the entire ZnO core although it accumulated more on the top of the nanowire. Figure 12 c) shows the zoom-in image of the nanowire tip. It shows that the diameter of core was about 100nm, and the CuO shell was rich on the top. Figure 12 d) is the diffraction pattern taken from the top of the core-shell nanowire. It shows the strong set of CuO (1-11) and (200) planes, which might suggest the single crystalline-like structure in the CuO tip. Figure 12 d) is the zoom-in image of body part of the core-shell nanowire. It shows that there was still a thin CuO shell layer covering the body part while CuO accumulateed on the top.

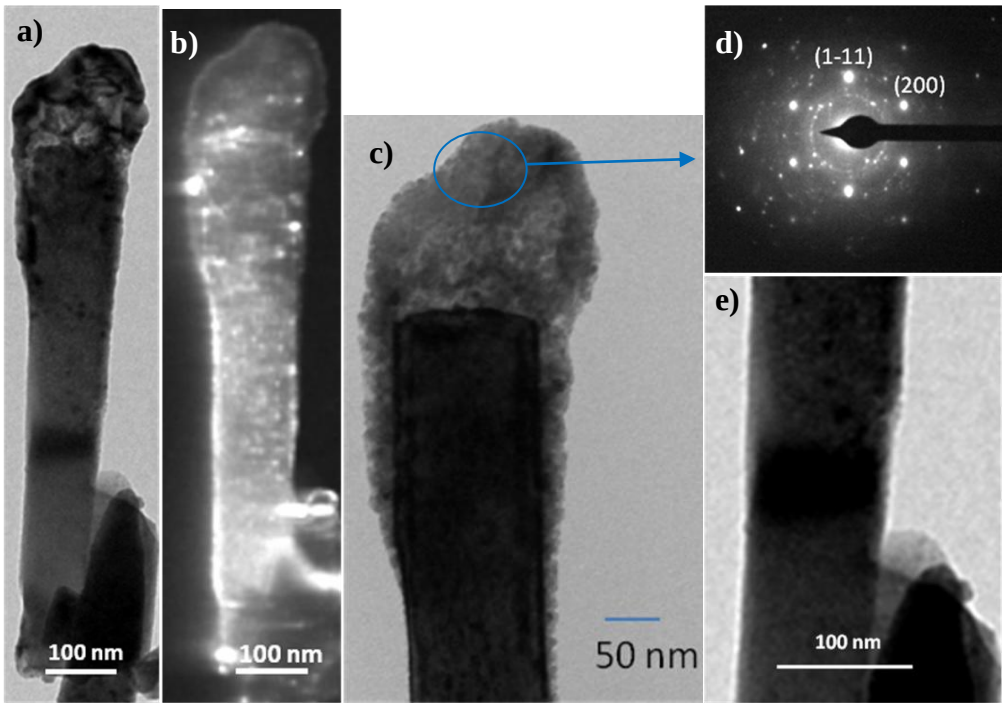

Figure 12. *TEM images of CuO/ZnO core- shell nanowire arrays grown at T=400 ℃,*

P=100mbar without oxygen flow.(S0) a) Bright field image of the ZnO/CuO core-shell nanowire. b) Dark field image of the ZnO/CuO core- shell nanowire. d) Diffraction pattern from the top portion of the ZnO/CuO core -shell nanowire. e) Zoom-in *image of body portion of the ZnO/CuO core-shell nanowire.*

Figure 12 shows the CuO/ZnO core-shell nanowire array growing at 400 ℃, 100 mbar with an oxygen flow rate of 50 sccm (S2). From Figure 12a), we can see that CuO/ZnO core-shell nanowire arrays successfully formed. From Figure 12 b), it clearly shows that CuO shell covered the entire ZnO core. A zoom-in dark field image (Figure 12 c) further revealed the formation of the core-shell CuO/ZnO nanowire. Figures 12 e)-f) display the diffraction patterns of the bottom of the CuO/ZnO core-shell nanowire. It indicates that ZnO grew along (0002) direction which was further proved in the following section by XRD results. Figure 12g) shows the diffraction pattern taken from the top shell of the CuO/ZnO core-shell nanowire. It shows the polycrystalline CuO despite of some strong diffraction spots in (002) and (202) planes.

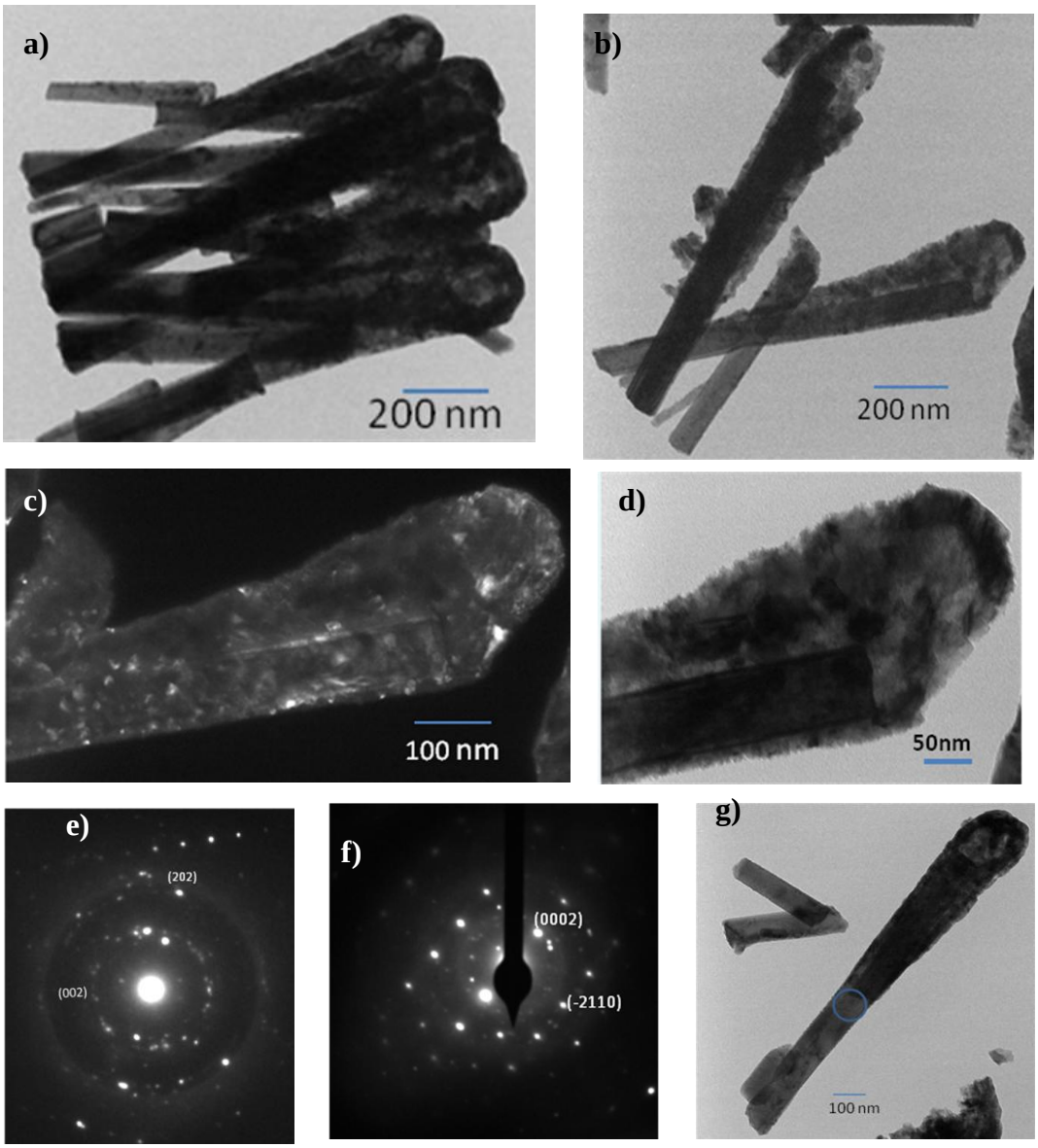

Figure 13. *TEM image of the CuO/ZnO core-shell nanowire array grown at T=400 °C, P=100mbar with 50 sccm Oxygen introducing.(S2) a),b)TEM images of CuO/ZnO core-shell nanowire arrays. c)Dark field image of the CuO/ZnO core-shell nanowire. d)Zoom-in top region of the CuO/ZnO core-shell nanowire. e) Diffraction pattern from the top portion of the CuO/ZnO core-shell nanowire f)g) Diffraction pattern of the bottom portion of the CuO/ZnO core-shell nanowire. .*

4.1.4 XRD

As previously described, CuO/ZnO core-shell nanowire arrays have been synthesized under different conditions. Their different phase structure and compositions will be discussed in this section. Spectrum (a) from as-grown ZnO

nanowires shows a strong peak at 34.8˚ that corresponds to (0002) plane (JCPD 89-0511, Hexagonal, a=3.249, c=5.205) as a result of ZnO nanowires' preferential growth direction along [0001] [15]. Spectrum (b) reveals the Cu peak at 43.3˚ that corresponds to (111) plane (JCPD 04-0836, Cubic, a=3.615), proving the successful deposition of Cu onto ZnO nanowires. Spectra (c), (d) and (e) display the XRD results from annealed samples with different growth conditions. It is clear that all three spectra contain a major common peak at 34.8˚ corresponding to (0002) peak of wurtzite ZnO nanowires, suggesting an intact ZnO nanowire core in the formed CuO-ZnO core-shell nanowire after various thermal annealing processes. Spectra (c) and (d) are both from samples annealed under 100mbar at 400℃. The only difference was with (50sccm, (d)) and without oxygen flow (0sccm, (c)). These two spectra both show two broad peaks at 35.5˚ and 38.8˚ which correspond to CuO (002)/(-111) and (111)/ (200) planes (JCPD 89-5899, Monoclinic, a=4.689, b=3.42, c=5.13, β=99.57) , respectively. The broadening of peaks might result from nano-sized CuO crystallines. Also, the intensity of these two peaks tended to be much stronger for sample under oxygen flow than sample without oxygen flow, suggesting that oxygen flow might enhance the degree of oxidation. Spectrum (e) shows the XRD pattern of sample annealed under 500mbar, a much higher pressure than the other samples. Two peaks at 33.9˚ and 36.4˚ were identified, which corresponds to Zn_2SiO_4 (211) (JCPD

24-1969, Orthorhombic, a=5.74, b=11.5, c=8.395) and Cu2O (111) (JCPD 78-2076, Cubic, a=4.267), respectively. $Zn_2SiO_4$4 might form at the interface of ZnO and Silicon substrates [55]. On the other hand, oxygen rich condition could favor the formation of CuO instead of Cu_2O, however, 3D nanoscale geometric effect might introduce a non-uniform distribution of O_2 partial pressure dependent on the local position, which may introduce non-homogeneous formation of oxides, i.e., a mixture of Cu_2O and CuO may form even at a high overall O_2 pressure on the top surface of nanorod arrays. In addition, the formation of Zn_2SiO_4 may play a role to reduce the access of oxygen for copper oxidation, which could lead to the formation of Cu_2O instead of CuO under 500 mbar, as indicated in the spectrum (e) in Figure 3.

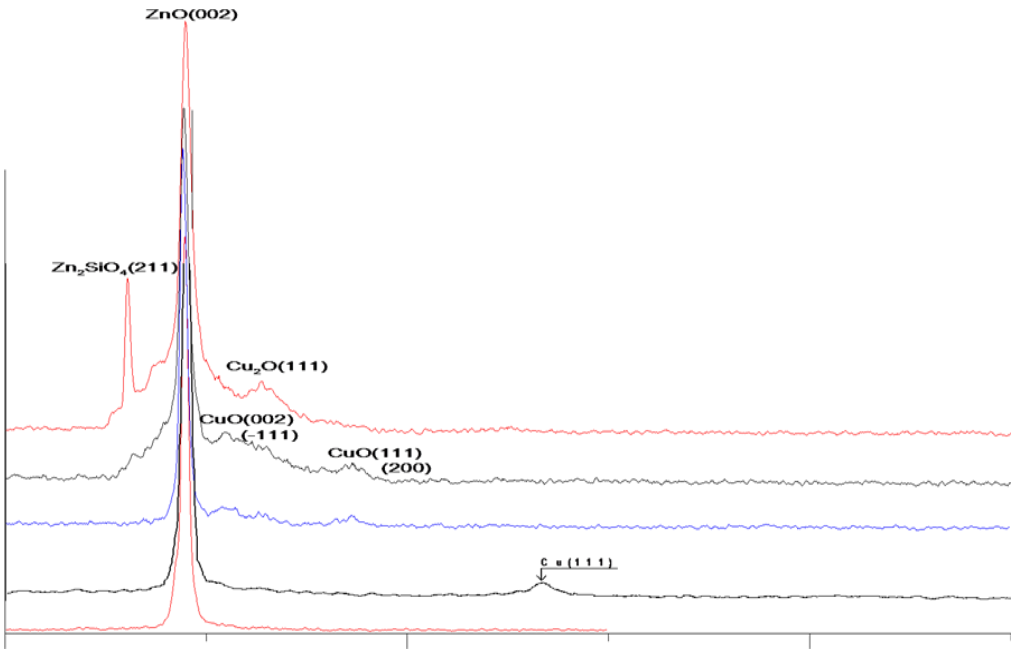

Figure 14. X-ray diffraction spectra of different nanowire samples *a)ZnO nanowires b) Cu/ZnO nanowires c) CuO/ZnO core-shell nanowire arrays growing at 400 °C and pressure 100mbar without oxygen flow. e) CuO/ZnO core-shell nanowire arrays growing at 400 °C and pressure 100mbar with 50*

sccm oxygen flow rate. f) CuO/ZnO core-shell nanowire arrays growing at 400 °C and pressure 500mbar with 50 sccm oxygen flow rate.

4.1.5 UV-Visible Absorption Spectroscopy

The optical property of this ZnO/CuO core-shell nanowire arrays has been characterized by UV-visible absorption spectroscopy. Since substrates with high absorption coefficient will hinder the information extraction of absorption spectrum corresponding to nanowire arrays, we investigated the absorption efficiency of ZnO/CuO core-shell nanowire arrays grown on quartz substrates instead of silicon substrates and used a blank quartz substrate as reference. Figure 15 shows the result of

absorption spectrum before and after forming the ZnO/CuO core-shell nanowire arrays.

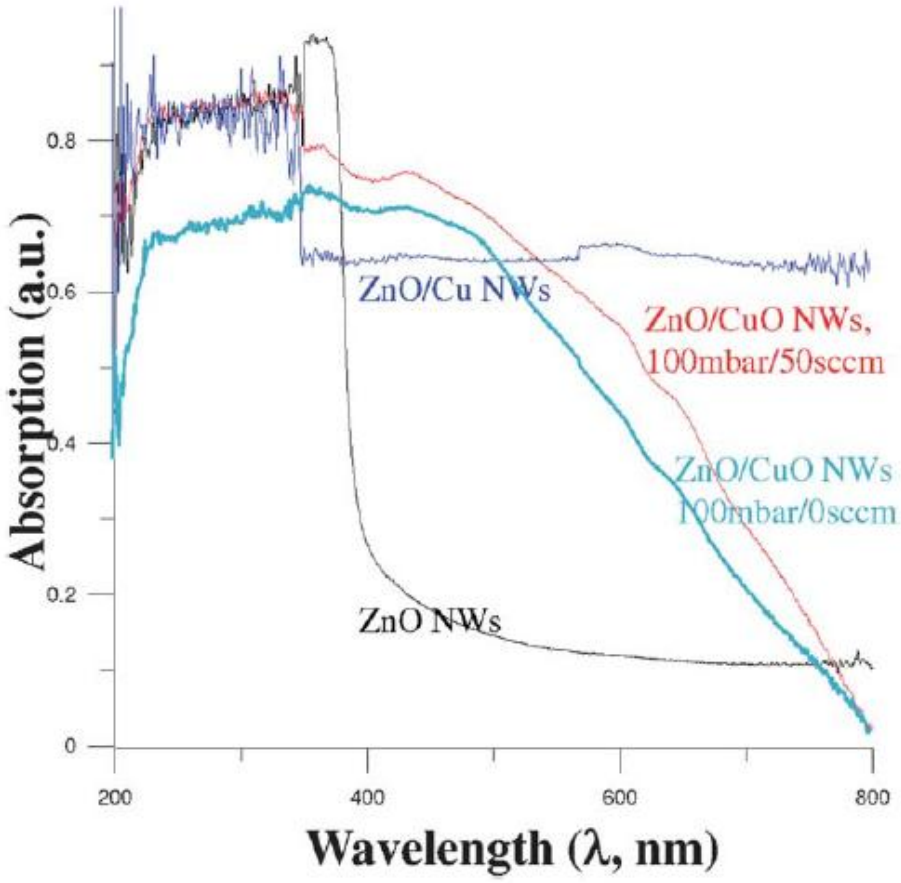

Figure 15 UV-vis absorption spectra of different nanowire samples.

It has been reported that ZnO with a direct band gap 3.3 eV has better absorption efficiency in UV region (200-380 nm)[56]. From Figure 15, one can see that pure ZnO nanowire arrays showed higher absorption efficiency from 200nm to 380nm and the absorbance droped dramatically in the visible region. It has been reported that CuO with a direct band gap 1.2eV have a wide absorption peak in the range 300nm to 600nm [57]. From Figure 15, ZnO/CuO core-shell nanowire arrays clearly showed higher absorption efficiency in the visible range (400-750 nm) as compared to pure ZnO nanowire arrays and had maximum absorption in the range 200nm to 400nm, which

might be resulted from both ZnO nanowires and band to band transition of CuO [58]. ZnO/CuO core-shell nanowire arrays also showed two broad peaks, respectively at 370nm, as predicted from the ellipsometry data [59], and 420nm, suggesting the possible success of CuO alloying onto ZnO nanowire arrays. In addition, because copper has strong absorption at a slightly lower energy, which results in orange color, Cu/ZnO nanowire arrays appear to increase absorption efficiency at higher wavelength. The small intensity increasing at around 560nm is suggested to be resulted from plasmonic resonance absorption [60].

4.2 Effective Factors of 3D Copper Thermal Oxidation

The mechanism of copper oxidation has been well documented since middle last century. While bulk copper and thin film might have different mechanisms, it has been found that during oxidation, Cu_2O tends to form first and CuO will form after sufficient oxidation time [44, 61, 62]. The chemical reactions take place in the following steps:

$2\ Cu + ½\ O_2 \rightarrow Cu_2O$

$Cu_2O + ½\ O_2 \rightarrow CuO$

Several different factors have been suggested that might affect copper oxidation, such as pressure, oxygen flow, annealing time, and temperature [63, 64]. However, the previous researches on Cu oxidation mainly focused on flat 2D film subjected to uniform oxygen pressure, while in this study, 3D ZnO nanowire arrays could play an important geometric effect on the copper oxidation behavior. In the following sections, we will discuss those possible factors controlling this unique 3D Copper oxidation behavior.

4.2.1 Effect of Pressure

It has been suggested that the variation of oxygen partial pressure could affect the morphology of the copper oxide scale formed though oxidation [65, 66]. In this study, different pressure was used to investigate the effect of forming ZnO/CuO core-shell nanowire arrays. Figure 16 shows a set of comparative SEM images of the formed ZnO/CuO nanowire arrays grown at 400 $^{\circ}C$ under either high pressure (1000mbar) or low pressure (100mbar). It shows that instead of core-shell nanowire arrays, under a pressure of 1000mbar, the CuO tended to grow in a form of thin film on top of the ZnO nanowire arrays, while when pressure decreased to 100mbar, the quality of ZnO/CuO core-shell nanowire arrays became much better, i.e., with a more conformal and uniform CuO coating surrounding individual ZnO nanowires. In higher pressure case, due to large oxidation rate at high pressure, fast Cu_xO substances fill-in occured

between adjacent ZnO-Cu nanowires, leading to drastically increasing barrier of the oxygen diffusion from the top portion to the bottom portion of nanowire arrays. This will lead to the dominant upward (↑) oxidation of Cu film, forming a relatively flat CuO nanofilm on top of ZnO nanowire arrays.

The previous section also compared the growth results at *400 ℃* with 50 sccm oxygen flow, and a variable pressure of either 500mbar or 100mbar, which further proves that low pressure will favor a conformal CuO thin film oxidation onto 3D ZnO nanowire arrays.

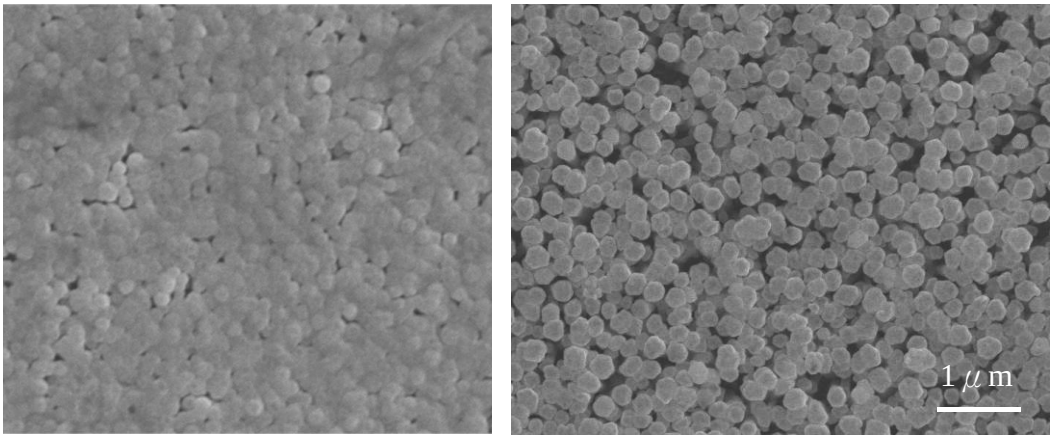

Figure 16 SEM images of *CuO/ZnO nanowires grown under two different conditions: Left: 400 ℃, 1000mbar; Right: 400 ℃, 100mbar.*

4.2.2 Discussion of Morphologies Barrier and Influence of Oxygen Flow

As discussed in previous section, through increasing oxygen flow rate, conformal Cu_xO thin-film is more likely to form surrounding individual ZnO nanowires. Since

S1, S2, and S3 were all under same pressure and temperature, i.e., 100mbar and 400 ℃, and prepumping for 1 hour before introducing the oxygen flow. Therefore, the oxygen partial pressure should be the same in the tube furnace according to ideal gas law:

PV=nRT

where P=pressure, V=volume, n=amount of substance, R=gas constant and T=temperature. The theory for the oxidation of flat copper thin film has suggested that with thickness roughly less than 40 nm, three steps will happen sequentially to define its oxidation mechanism. [67-71]

1. Oxidant absorbed on the surface of oxide/ metal.
2. Due to good electron affinity of oxygen, electrons will diffuse through oxidant by tunneling effect or thermioic emission to form O-, which built up an electric field between Cu ion and O-.
3. Cu ion will migrate to form the copper oxide layer since copper diffuses much faster than oxygen.

However, previous researches generally focus on flat 2D thin film with uniform oxygen pressure, while in this study, 3D nanowire arrays' geometrical effect on the copper oxidation needs to be taken into consideration. Comparing samples with and without oxygen flow from Figure 17, both SEM and TEM images show that the

sample with oxygen flow will result in more thorough growth of copper oxide shell layer.

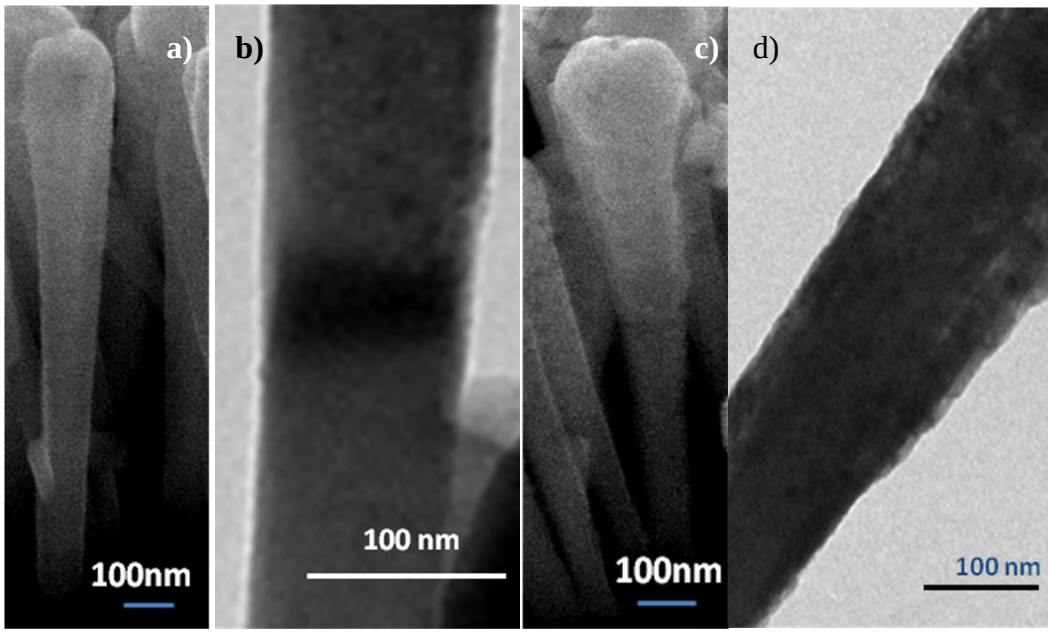

Figure 17 a) SEM image of Sample(S0) grown at pressure 100mbar without oxygen flow. b) TEM zoom in image of body portion of the Sample(S0) and c) SEM image of the Sample(S2) grown at pressure 100mbar with 50 sccm oxygen flow. d) TEM zoom in image of body portion of the Sample(S2) reveals the formation of core-shell structure.

This suggested that without oxygen flow, due to the dense packing of Cu/ZnO nanowires in the array form, very limited amount of oxygen will be accessed at the bottom portion of nanowire. Therefore, drastically more oxygen access is possible on the nanowire top surface than the bottom portion, leading to the formation of none–uniform and non-conformal CuO nanofilm grown on ZnO nanowire arrays. To understand the microscopic mechanism in unique Cu oxidation behavior on the 3D nanowire arrays, a simple electrical field model is proposed here. Here, we can simplify the Cu/ZnO nanowires morphologies into two parts, top portion as sphere

and body portion as cylinder, then consider a single copper ion located at the boundary of top and body portion as the Figure 18 a) shows.

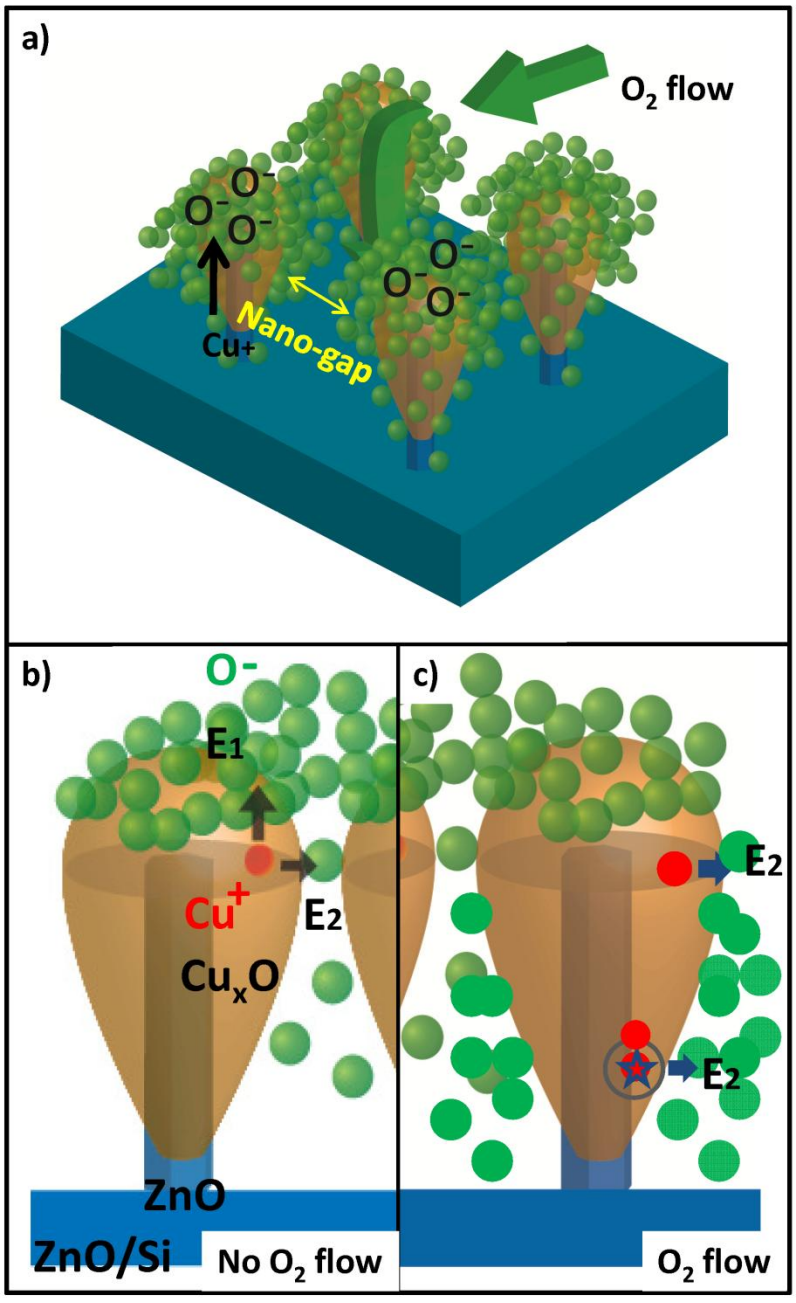

Figure 18 Schematic diagrams of proposed microscopic mechanism for the formation of ZnO-CuO core-shell nanowires. (a) Schematic of Cu ion location and oxygen flow. (b) Dominant Cu ion's upward (↑) diffusion in absence of oxygen flow. (c) Outward (→) diffusion of Cu ion with oxygen flow; star: Cu ion migration induced vacancy, filled by downward migration and fill-in of Cu ions from above.

If oxygen content is richer on the top portion (semi-sphere), the built-in upward (↑) electrical field (E1) will be stronger than the outward (→) electrical field in the body portion (E2), which will result in a dominant copper ion's diffusion upward instead of outward diffusion towards shell, as Figure 18 b) showed. *When introducing oxygen flow*, the difference between oxygen local partial pressure at the top of sample and the bottom of sample might be large enough to conquer the geometric diffusion barrier of oxygen caused by the unique 3D morphology. In this case, oxygen will then diffuse into the bottom as shown in Figure 18 c), resulting in more oxidant permeating into the bottom portion of the nanowires, inducing better coverage of copper oxide film surrounding core ZnO nanowires.

4.2.3 Copper Ion Anisotropic Transport Rate

Besides the pressure, morphologies barrier, and introducing of oxygen flow rate, the other possible reason that might result in the unique copper oxidation behavior is anisotropic oxidation rate of copper. It has been indicated that copper will have different oxidation rates at different crystal faces. [76]Also, for nanoscale copper oxidation behavior, effective diffusion coefficient may need to be modified due to the fact that copper ions might diffuse along the grain boundaries. Therefore, the effective diffusion coefficient should be modified to

$D_{eff} = (1-f)D_L + fD_B$,

Where D_L is the lattice diffusion coefficient and D_B is the grain boundary diffusion coefficient. *f* is the fraction of the total number of diffusion sites located in the boundaries. When the grain diameter is very small, D_{eff} will be dominated by D_B.[77] However, analyzing the surface crystallography and structure on the micro-scale is very difficult, but it is for sure, nano-scale copper oxidation will be different from bulk oxidation behavior. Further investigation are being conducted to help further unravel this anisotropic oxidation effect, which is potentially very useful for designing and enabling unique nanoscale building blocks for desired structure and functional applications.

4.3 Summary

Thermal oxidation of Cu nanofilm on the 3D ZnO nanowire arrays has been tuned by introducing different oxygen flow rates. It is suggested that increasing oxygen flow rate might help increase local partial oxygen pressure, resulting in the increasing degree of oxidation throughout each ZnO/Cu single nanowire. Higher pressure might favor in the formation of Zn_2SiO_4 at the interface of ZnO and Silicon substrates. ZnO/CuO core-shell nanowire arrays have demonstrated better absorption efficiency in visible region compared to pure ZnO nanowire arrays, which suggests a good potential for ZnO/CuO core-shell nanowire arrays as nanoscale building blocks

in solar cells and light emission devices.

Chapter 5 Conclusion and Future Directions

Based on the experimental results and discussions elaborated in the chapters 2-4, a few conclusions can be drawn for this thesis work:

1. Large scale ZnO/CuO core-shell nanowire arrays have been successfully synthesized onto silicon substrates by a simple three-step sequential process including the hydrothermal synthesis of ZnO nanowire arrays, Cu-sputtering on ZnO nanowire arrays, and thermal oxidation of ZnO/Cu nanowire arrays.

2. The effect of pre-annealing condition of ZnO seed layer was systematically studied on the growth of ZnO nanowire arrays. It shows that seed layer could lead to more uniform and well-aligned ZnO nanowires. In addition, increasing of annealing time and thickness of seed layer will help increase ZnO nanowire's diameter.

3. The grown ZnO nanowire arrays were well aligned with a preferential growth direction along [0002]. With the increase of diameter and density of Cu/ZnO nanowire arrays, Cu/ZnO nanowires tended to form nail shaped morphology. Thermal oxidation of Cu nanofilm on the 3D as-grown ZnO nanowire arrays has been tuned by adjusting oxidation oxygen flow rate and pressure. On the copper oxidation, a copper ion migration model has suggested that copper ions will diffuse into vacancy sites instead of oxygen ions. Due to the dense packing of Cu/ZnO nanowire arrays, very

limited amount of oxygen might exist on the bottom portion of Cu/ZnO nanowire arrays without inputting oxygen flow, which resulted in the formation of non-uniform ZnO/CuO core-shell nanowire arrays. On the other hand, with oxygen input, increasing oxygen flow rate might result in much more difference of local partial oxygen pressure between the top portion and the bottom portion of Cu/ZnO nanowire arrays, which can help conquer the barrier of oxygen diffusion into the bottom. The degree of oxidation conformality throughout each single ZnO/Cu nanowire hence increased, resulting in more uniform ZnO/CuO core-shell nanowire arrays. In addition, both XRD and TEM showed that CuO would form either with or without oxygen flow under lower pressure (100mbar) at 400℃. Higher pressure, however, might favor the formation of Zn_2SiO_4 at the interface of ZnO and Si substrates and result in poor quality of CuO thin film on top of ZnO nanowire arrays.

4. ZnO with a band gap ~3.3 eV at room temperature has a higher absorption efficiency at wavelength ~200nm- 380nm. Compared to ZnO, CuO has a much smaller band gap around 1.2 eV, with a much higher absorption efficiency at wavelength ~300nm- 600 nm. Thus, ZnO/CuO core-shell nanowire arrays have exhibited much better absorption efficiency in visible region compared to pure ZnO nanowire arrays experimentally.

In short, Cu nanofilm oxidation behavior onto a unique 3D ZnO nanowire array

have been studied by tuning oxygen flow and pressure during the thermal oxidation process. Comparing with previous studies, [78-80] by introducing oxygen flow and lower pressure, we achieved more thorough CuO shell layer surrounding ZnO nanowire core by a simple low temperature thermal oxidation. It also suggested the good feasibility to well control the morphology and quality of the core-shell nanomaterials using simple thermal oxidation. This mechanism behind may be extended to other binary core-shell semiconductor oxide systems to achieve better quality core-shell nanowire arrays through this simple thermal oxidation method.

ZnO/CuO core-shell nanowire arrays may have good potential to be used as nanoscale building blocks in solar cells and light emission devices since it may broaden utilizing solar absorption spectrum. Further electrical and optical characterization of this ZnO/CuO core-shell nanowire arrays need to be conducted in the near future in order to apply it into the photovoltaic devices.

References

1. G. John, *Richard Feynman: A Life in Science,* Dutton 1997 170

2. R. R. Allison, H. C. Mota, V. S. Bagnato and C. H. Sibata, Photodiagnosis and Photodynamic Therapy 5, 19 (2008).

3. O. M. Koo, Israel Rubinstein and Hayat Onyuksel, Nanomedicine: Nanotechnology, Biology and Medicine 1, 193 (2005).

4. W. A. Tisdale, K. J. Williams, B. A. Timp, D. J. Norris, E. S. Aydil and X. -Y Zhu, Science 328, 1543 (2010).

5. S. -L Jeng, J. -C Lu and K. Wang, IEEE Trans. Reliab. 56, 401 (2007).

6. Guozhong Gao, NANOSTRUCTURE & NANOMATERIALS SYTHESIS, PROPERTIES & APPLICATION, Imperial College Press (2004)7. S. Iijima, Proceedings of the IEEE Micro Electro Mechanical Systems (MEMS) 520 (1998).

8. C. N. R. Rao, A. Muller, A.K. Cheetham, The Chemisry of Nanomaterials: Synthesis, Properties and Applications, Wiley-VCH (2005),

9. A. I. Hochbaum, R. Fan, R. He and P. Yang, Nano Letters 5, 457 (2005).

10. Y. Wu, R. Fan and P. Yang, Nano Letters 2, 83 (2002).

11. J. D. Holmes, K. P. Johnston, R. C. Doty and B. A. Korgel, Science 287, 1471 (2000).

12. P. Shimpi, P. -X Gao, D. G. Goberman and Y. Ding, Nanotechnology 20, 125608 (2009).

13. P. Reiss, M. Protière and L. Li, Small 5, 154 (2009).

14. Y. Zhang, L. -W Wang and A. Mascarenhas, Nano Letters 7, 1264 (2007).

15. Z. L. Wang, Journal of Physics Condensed Matter 16, R829 (2004).

16. Ü. Özgür, Ya I. Alivov, C. Liu, A. Teke, M. A. Reshchikov, S. Doğan, V. Avrutin, S. -J Cho and H. Morko¸, J. Appl. Phys. 98, 1 (2005).

17. G. Zou, H. Li, Y. Zhang, K. Xiong and Y. Qian, Nanotechnology 17, S313 (2006).

18. S. Baruah and J. Dutta, Science and Technology of Advanced Materials 10, 013001 (2009).

19. T. Ohgaki, N. Ohashi, S. Sugimura, H. Ryoken, I. Sakaguchi, Y. Adachi and H. Haneda, J. Mater. Res. 23, 2293 (2008).

20. S. -M Zhou, X. -H Zhang, X. -M Meng, K. Zou, X. Fan, S. -K Wu and S. -T Lee, Nanotechnology 15, 1152 (2004).

21. J. H. Kim, H. Kim, D. Kim, S. G. Yoon and W. K. Choo, Solid State Commun. 131, 677 (2004).

22. T. -J Hsueh, C. -L Hsu, S. -J Chang, P. -W Guo, J. -H Hsieh and I. -C Chen, Scr. Mater. 57, 53 (2007).

23. J. Cui and U. J. Gibson, Journal of Physical Chemistry C 114, 6408 (2010).

24. Y. Zhu, C. -H Sow, T. Yu, Q. Zhao, P. Li, Z. Shen, D. Yu and J. T. -L Thong, Advanced Functional Materials 16, 2415 (2006).

25. B. Balamurugan and B. R. Mehta, Thin Solid Films 396, 90 (2001).

26. J. B. Forsyth and S. Hull, Journal of Physics: Condensed Matter 3, 5257 (1991).

27. H. Matsumura, A. Fujii and T. Kitatani, Japanese Journal of Applied Physics, Part 1: Regular Papers and Short Notes and Review Papers 35, 5631 (1996).

28. K. Zamani, proc. SPIE 4068, 266 (2002).

29. B. Tian, X. Zheng, T. J. Kempa, Y. Fang, N. Yu, G. Yu, J. Huang and C. M. Lieber, Nature 449, 885 (2007).

30. M. A. Green, J. Mater. Sci. : Mater. Electron. 18, 15 (2007).

31. C. Xu, P. Shin, L. Cao and D. Gao, Journal of Physical Chemistry C 114, 125 (2010).

32. B. M. Kayes, H. A. Atwater and N. S. Lewis, J. Appl. Phys. 97, 1 (2005).

33. R. Behrisch, Sputtering by Particle bombardment, Springer-Verlag (1981).

34. M. Wang, C. Huang, Y. Cao, Q. Yu, W. Guo, Q. Liu, J. Liang and M. Hong, Nanotechnology 20, 285311 (2009).

35. De Lodyguine JS. Illuminant for incandecent lamps. US patent 575002, (1893).

36. D. Kim, P. Shimpi and P. -X Gao, Nano Research 2, 966 (2009).

37. K. L. Choy, Progress in Materials Science 48, 57 (2003).

38. Byrappa K and Yoshimura M, Handbook of Hydrothermal Technology, Noyes Publications/ William Andrew Publishing, LLC (2001).

39. L. E. Greene, B. D. Yuhas, M. Law, D. Zitoun and P. Yang, Inorg. Chem. 45, 7535 (2006).

40. J. Qiu, X. Li, W. He, S. -J Park, H. -K Kim, Y. -H Hwang, J. -H Lee and Y. -D Kim, Nanotechnology 20, 155603 (2009).

41. G. Honjo, Journal of the Physical Society of Japan 4, 330 (1949).

42. J. Bardeen, W. H. Brattain and W. Shockley, J. Chem. Phys. 14, 714 (1946).

43. T. N. Rhodin Jr., J. Am. Chem. Soc. 72, 5102 (1950).

44. A. O. Musa, T. Akomolafe and M. J. Carter, Solar Energy Mater. Solar Cells 51, 305 (1998).

45. W. Gao, H. Gong, J. He, A. Thomas, L. Chan and S. Li, Mater Lett 51, 78 (2001).

46. L. Vayssieres, Adv Mater 15, 464 (2003).

47. M. Izaki, T. Shinagawa, K. -T Mizuno, Y. Ida, M. Inaba and A. Tasaka, J. Phys. D 40, 3326 (2007).

48. K. Akimoto, S. Ishizuka, M. Yanagita, Y. Nawa, G. K. Paul and T. Sakurai, Solar Energy 80, 715 (2006).

49. H. Tanaka, T. Shimakawa, T. Miyata, H. Sato and T. Minami, Appl. Surf. Sci. 244, 568 (2005).

50. S. S. Jeong, A. Mittiga, E. Salza, A. Masci and S. Passerini, Electrochim. Acta 53, 2226 (2008).

51. S. Xu, N. Adiga, S. Ba, T. Dasgupta, J. Wu and Z. L. Wang, ACS Nano 3, 1803 (2009).

52. L.-W Ji, S.-M Peng, J.-S Wu, W.-S Shih, C.-Z Wu and I.-T Tang, Journal of Physics and Chemistry of Solids 70, 1359 (2009).

53. Y.-HKang, C.-G Choi, Y.-S Kim and J.-K Kim, Mater Lett 63, 679 (2009).

54. D. C. Kim, B. H. Kong, H. K. Cho, D. J. Park and J. Y. Lee, Nanotechnology 18, 015603 (2007).

55. P. Shimpi, Y. Ding, E. Suarez, J. Ayers and P. -X Gao, Appl. Phys. Lett. 97, (2010).

56. Y. -H Ni, X. -W Wei, J. -M Hong and Y. Ye, Materials Science and Engineering B: Solid-State Materials for Advanced Technology 121, 42 (2005).

57. X. Y. Chen, H. Cui, P. Liu and G. W. Yang, Appl. Phys. Lett. 90, (2007).

58. J. Liu, X. Huang, Y. Li, K. M. Sulieman, X. He and F. Sun, Journal of Materials Chemistry 16, 4427 (2006).

59. H. Amekura, N. Umeda, Y. Takeda and N. Kishimoto, Appl. Phys. Lett. 89, (2006).

60. O. Vázquez-Cuchillo, U. Pal and C. Vázquez-Lopez, Solar Energy Mater. Solar

Cells 70, 369 (2001).

61. M. O'Reilly, X. Jiang, J. T. Beechinor, S. Lynch, C. NíDheasuna, J. C. Patterson and G. M. Crean, Appl. Surf. Sci. 91, 152 (1995).

62. D. L. Cocke, R. Schennach, M. A. Hossain, D. E. Mencer, H. McWhinney, J. R. Parga, M. Kesmez, J. A. G. Gomes and M. Y. A. Mollah, Vacuum 79, 71 (2005).

63. A. Kumar, A. K. Srivastava, P. Tiwari and R. V. Nandedkar, Journal of Physics Condensed Matter 16, 8531 (2004).

64. C. H. Xu, C. H. Woo and S. Q. Shi, Superlattices and Microstructures 36, 31 (2004).

65. A. G. Nasibulin, O. Richard, E. I. Kauppinen, D. P. Brown, J. K. Jokiniemi and I. S. Altman, Aerosol Science and Technology 36, 899 (2002).

66. C. H. Xu, C. H. Woo and S. Q. Shi, Superlattices and Microstructures 36, 31 (2004).

67. N. Cabrera and N. F. Mott, Reports on Progress in Physics 12, 163 (1949).

68. W. Gao, H. Gong, J. He, A. Thomas, L. Chan and S. Li, Mater Lett 51, 78 (2001).

69. Z. Han, L. Lu, H. W. Zhang, Z. Q. Yang, F. H. Wang and K. Lu, Oxidation Metals 63, 261 (2005).

70. R. Nakamura, D. Tokozakura, H. Nakajima, J. -G Lee and H. Mori, J. Appl. Phys. 101, (2007).

71. D. DeNardis, D. Rosales-Yeomans, L. Borucki and A. Philipossian, Thin Solid Films 518, 3903 (2010).

72. I. Platzman, R. Brener, H. Haick and R. Tannenbaum, Journal of Physical Chemistry C 112, 1101 (2008).

73. T. Ma, M. Guo, M. Zhang, Y. Zhang and X. Wang, Nanotechnology 18, 035605 (2007).

74. S. -Y Liu, T. Chen, J. Wan, G. -P Ru, B. -Z Li and X. -P Qu, Applied Physics A: Materials Science and Processing 94, 775 (2009).

75. J. Song and S. Lim, Journal of Physical Chemistry C 111, 596 (2007).

76. T. N. Rhodin Jr., J. Am. Chem. Soc. 73, 3143 (1951).

77. Z. Han, L. Lu, H. W. Zhang, Z. Q. Yang, F. H. Wang and K. Lu, Oxidation Metals 63, 261 (2005).

78. et al Sungmook Jung, Nanotechnology 22, 015606 (2011).s

79. X. Zhao, P. Wang and B. Li, Chemical Communications 46, 6768 (2010).

80. T. -J Hsueh, C. -L Hsu, S. -J Chang, P. -W Guo, J. -H Hsieh and I. -C Chen, Scr. Mater. 57, 53 (2007).